Reproduction of correct electrostatic field by charges and dipoles on a closed surface

Haruki Nakamura

Protein Engineering Research Institute, Osaka, Japan

A general algorithm based on the Green function theorem has been developed to correctly reproduce electrostatic fields inside a closed space by point charges and point dipoles on the surface surrounding the space. For actual computations, limited numbers of point charges, including charge pairs replacing point dipoles, are enough to approximate the inner fields. As examples, reaction fields were reproduced by the current surface charges and dipoles for the dielectric models, where a monopole, dipole, or quadrupole was individually set at the center in a vacuum sphere surrounded by high dielectric continuum. The potentials due to those reaction fields agree well with the analytical ones. As an application of this method to the analysis of the electronic structure of the active site of a protein, a combination of the continuum dielectric model and ab initio *molecular orbital calculation was carried out. Other applications to molecular dynamics and quantum mechanical calculations are also discussed.*

Keywords: electrostatic potential, surface charges and dipoles, Green function, macroscopic dielectric model, ab initio *MO calculation*

INTRODUCTION

Specific molecular recognitions and enzymatic reactions are essential functions of proteins, which have long been subjects to be revealed experimentally and theoretically. It is recognized that electrostatic properties of proteins should be well understood from theoretical analyses for those problems.[1] Since proteins in solvent or in membrane are very dynamic and heterogeneous from an electrostatic viewpoint, the inner electrostatic fields cannot be quantified simply.

Macroscopic dielectric models have been numerically solved for those heterogeneous systems,[2,3] and several experimental electrostatic properties have been explained well by this kind of analysis.[4–6] However, the macroscopic model is essentially static, and the dynamic properties of the system are parameterized as the "local dielectric constant," which is a physically confusing concept.[7] That is, the macroscopic model is only useful for obtaining electrostatic fields due to charges and dipoles in an averaged fashion. For a more detailed discussion, the author has developed the PPPM (PP, particle–particle; and PM, particle–mesh) algorithm,[8] which was used in plasma simulations.[9] In the PPPM scheme, the total electrostatic potential is a sum of the analytical Coulombic potential (PP) and the other smooth potential due to the reaction field, which numerically is given as a mesh potential (PM). By this treatment, not only is better accuracy obtained than from the conventional macroscopic dielectric model, but also a dynamic calculation is possible with the mesh potential.[8]

For the analysis of the electronic structure of the active sites of proteins, quantum mechanical (QM) calculations with the electrostatic contribution from the whole protein and the solvent should be carried out.[10–15] Recently, combined approaches of QM and molecular dynamics (MD) calculations have been developed to reveal the mechanisms of chemical reactions in solution.[16,17] In those cases, simulations of solvent molecules cannot be rejected to incorporate their shielding effects correctly. However, such calculations need enormous computation time just for calculations of solvent molecules.

In the present article, a new method has been developed to correctly reproduce any electric field without singular points inside a closed surface, by point charges and point dipoles on the closed surface. This method is suitable for ordinary QM calculations, and it becomes possible to compute a more realistic electronic structure of the active site of a protein in aqueous solution than before.

METHODOLOGY

As a basis of the electromagnetic theorem, the electrostatic potential φ at the position $\mathbf{r}$ obeys a Poisson equation;

$$\nabla^2\varphi(\mathbf{r}) = \frac{-4\pi\rho(\mathbf{r})}{\epsilon_0} \tag{1}$$

where $\rho(\mathbf{r})$ is the electron density at position $\mathbf{r}$, and ϵ_0 is the dielectric constant. If the position $\mathbf{r}$ is inside a closed surface

Color Plates for this article are on page 43.

Address reprint requests to Dr. Nakamura, Protein Engineering Research Institute, 6-2-3 Furuedai, Suita, Osaka 565, Japan.
Received 10 December 1991; accepted 28 January 1992

Γ, φ can be divided into the two functions φ_i and φ_0;

$$\varphi = \varphi_i + \varphi_0 \tag{2}$$

$$\nabla^2\varphi_i(\mathbf{r}) = \frac{-4\pi\rho(\mathbf{r})}{\epsilon_0} \tag{3}$$

$$\nabla^2\varphi_0(\mathbf{r}) = 0 \tag{4}$$

Here, φ_i is the electrostatic potential due to charge sources inside Γ, and φ_0 is due to those outside of Γ, including the reaction field. Since Equation 4 is a Laplace equation, the solution is generally described from Green's theory;

$$\varphi_0(\mathbf{r}) = \frac{\epsilon_0}{4\pi}\int_\Gamma (\nabla\varphi_0(\mathbf{r}')\cdot\mathbf{n})\, G(\mathbf{r}|\mathbf{r}') - \varphi_0(\mathbf{r}')\,(\nabla G(\mathbf{r}|\mathbf{r}')\cdot\mathbf{n})\, dS(\mathbf{r}') \tag{5}$$

In Equation 5, the integration should be carried out on the surface of Γ and $\mathbf{n}$ is a unit vector, which points outwards to a normal of the surface Γ. $G(\mathbf{r}|\mathbf{r}')$ is a Green function, which satisfies the following equation at any position inside the closed surface Γ:

$$\nabla^2 G(\mathbf{r}|\mathbf{r}') = \frac{-4\pi\delta(\mathbf{r}-\mathbf{r}')}{\epsilon_0} \tag{6}$$

Since there is no singular point inside Γ with a uniform dielectric constant ϵ_0, or *in vacuo*, the next simple function is available as the Green function.

$$G(\mathbf{r}|\mathbf{r}') = (\epsilon_0|(\mathbf{r}-\mathbf{r}')|)^{-1} \tag{7}$$

Then, Equation 5 is rewritten as follows:

$$\varphi_0(\mathbf{r}) = \int_\Gamma \frac{[\epsilon_0(\nabla\varphi_0(\mathbf{r}')\cdot\mathbf{n})/4\pi]}{\epsilon_0|(\mathbf{r}-\mathbf{r}')|}\, dS(\mathbf{r}') + \int_\Gamma \frac{[-\epsilon_0(\varphi_0(\mathbf{r}')\mathbf{n})/4\pi]\cdot(\mathbf{r}-\mathbf{r}')}{\epsilon_0|(\mathbf{r}-\mathbf{r}')|^3}\, dS(\mathbf{r}') \tag{8}$$

The physical meaning of Equation 8 is very simple. The first integration indicates the sum of the electrostatic potentials due to the pseudo-point charges $dQ(\mathbf{r}')$, and the second is the sum of the potentials due to the pseudo-point dipoles $d\mu(\mathbf{r}')$ on the surface Γ, described, respectively, as:

$$dQ(\mathbf{r}') = \epsilon_0(\nabla\varphi_0(\mathbf{r}')\cdot\mathbf{n})\, dS/4\pi \tag{9}$$

$$d\mu(\mathbf{r}') = -\epsilon_0(\varphi_0(\mathbf{r}')\mathbf{n})\, dS/4\pi \tag{10}$$

Thus, once the potentials $\varphi_0(\mathbf{r}')$ and their gradients $\nabla\varphi_0(\mathbf{r}')$ on the closed surface Γ are obtained, the electrostatic potential at any position inside Γ can be given by taking the sum of the potentials φ_i due to the actual charge sources inside Γ and the potential φ_0 due to the pseudo-charges and dipoles on Γ.

To calculate Equation 8 numerically, an arbitrarily chosen closed surface is divided into lots of small areas ΔS_k (k = 1, 2, . . . , N). Instead of the integrations in Equation 8, discrete sums are taken:

$$\varphi_0(\mathbf{r}) = \sum_{k=1}^{N} \Delta Q_k/(\epsilon_0|(\mathbf{r}-\mathbf{r}'_k)|) + \sum_{k=1}^{N} \Delta\mu_k\cdot(\mathbf{r}-\mathbf{r}'_k)/(\epsilon_0|(\mathbf{r}-\mathbf{r}'_k)|^3) \tag{11}$$

where $\mathbf{r}'_k$ is the center of the kth surface area. Here, replacing Equations (9) and (10), the discrete charges and dipoles located at $\mathbf{r}'_k$ are considered.

$$\Delta Q_k = \epsilon_0(\nabla\varphi_0(\mathbf{r}'_k)\cdot\mathbf{n})\,\Delta S_k/4\pi \tag{12}$$

$$\Delta\mu_k = -\epsilon_0(\varphi_0(\mathbf{r}'_k)\mathbf{n})\,\Delta S_k/4\pi \tag{13}$$

Each point dipole of Equation 13 can be replaced by a charge pair, ΔQ_k^+ and ΔQ_k^-, located at $\mathbf{r}'_k + \Delta l\mathbf{n}/2$ and $\mathbf{r}'_k\Delta l\mathbf{n}/2$, respectively, without losing precision as mentioned later;

$$\Delta Q_k^+ = |\Delta\mu_k(\mathbf{r}'_k)|/\Delta l \tag{14}$$

$$\Delta Q_k^- = -|\Delta\mu_k(\mathbf{r}'_k)|/\Delta l \tag{15}$$

Here, Δl is the artificial distance between the charge pair, taking a very short length. Then, the electrostatic potential inside Γ due to the outside of Γ is calculated numerically from only $3 \times N$ pseudo-charges, ΔQ_k, and charge pairs, ΔQ_k^+ and ΔQ_k^-:

$$\varphi_0(\mathbf{r}) = \sum_{k=1}^{N} \Delta Q_k/(\epsilon_0|(\mathbf{r}-\mathbf{r}'_k)|) + \sum_{k=1}^{N} \Delta Q_k^+/(\epsilon_0|\mathbf{r}-(\mathbf{r}'_k+\Delta l\mathbf{n}/2)|) + \sum_{k=1}^{N} \Delta Q_k^-/(\epsilon_0|\mathbf{r}-(\mathbf{r}'_k-\Delta l\mathbf{n}/2)|) \tag{16}$$

RESULTS

Reproduction of the reaction fields

For simple cases where Equations 2/4 are applied, the reaction fields in simple dielectric models were considered. Unit charges were set approximating a monopole, a dipole, and a quadrupole around the center of a vacuum sphere (of radius R_s = 16 Å, where 1Å = 0.1 nm, and the dielectric constant is ϵ_0 = 1) in an aqueous solvent (dielectric constant ϵ_s = 80). For a monopole, a unit charge was set at the center of the vacuum sphere ($X = Y = Z = 0$). For a dipole, two unit charges $+e$ and $-e$ were positioned on the X-axis at X = 1 Å and − 1 Å, respectively. For a quadrupole, two positive unit charges $+e$ were set on the X-axis at $X = \pm 1$ Å, and two negative unit charges $-e$ were on the Y-axis at $Y = \pm 1$ Å. As a closed surface Γ, a 10-Å radius sphere was considered in the vacuum sphere with the same center position. Then, in each model, φ_i is a potential *in vacuo* due to the direct contribution from the charge sources, and φ_0 is the potential due to their reaction field.

The reaction field potential was first analytically calculated, using the Friedman's equation (Equations 6 and 7 of Friedman[18]) with the zeroth, first and second terms, at any position in the vacuum sphere. At the same time, the reaction field potential and its gradient for the finite numbers of the points on Γ were calculated in the same way. From those values on Γ, the pseudo-charges and dipoles were obtained following Equations 12 and 13, and the reaction field potentials were reproduced by Equation 11. Instead of using Equation 13, Equations 14 and 15 were also used to reproduce the reaction field potential, through Equation 16.

Figures 1a and 1b show the original and the reproduced

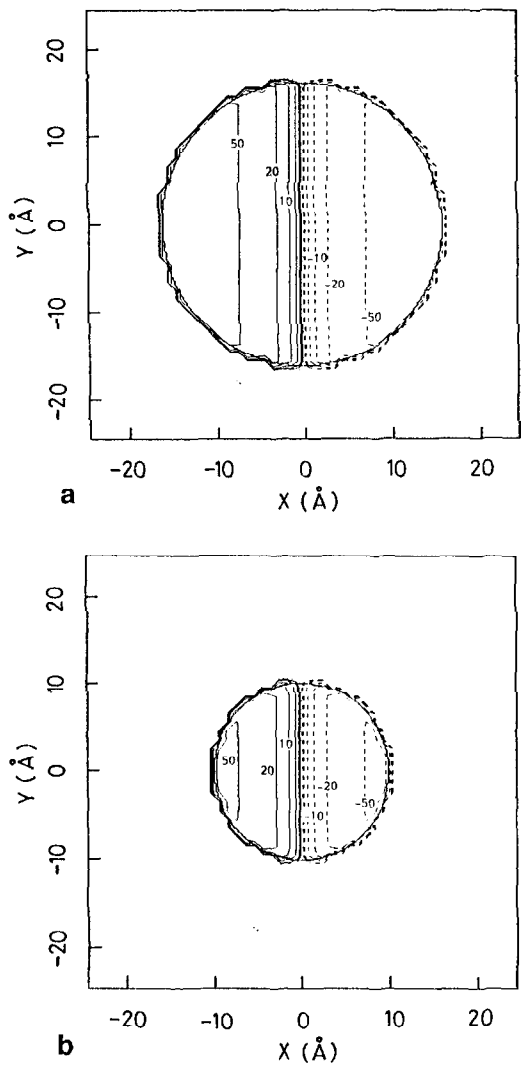

Figure 1. Electrostatic equipotential lines due to the reaction field in the cross section at Z = 0.5 Å *for a dipolar dielectric model, where two unit charges* +e *and* −e *were positioned on the* X*-axis at* X = +1 Å *and* −1 Å, *respectively, in a 16-Å vacuum sphere surrounded by a high dielectric continuum (dielectric constant 80). The solid lines indicate positive potential values and the dashed lines represent negative values. The numbers in the figures indicate the potential values (in mV):* (a) *The analytical result by the Friedman's equation.*[18] *The bold line is the surface of the vacuum sphere.* (b) *The reproduced potential by the 3 × 1282 pseudo-charges and charge pairs on the closed surface* Γ *(10-Å sphere) with* $\Delta l = 10^{-4}$ Å. *The bold line indicates the surface* Γ.

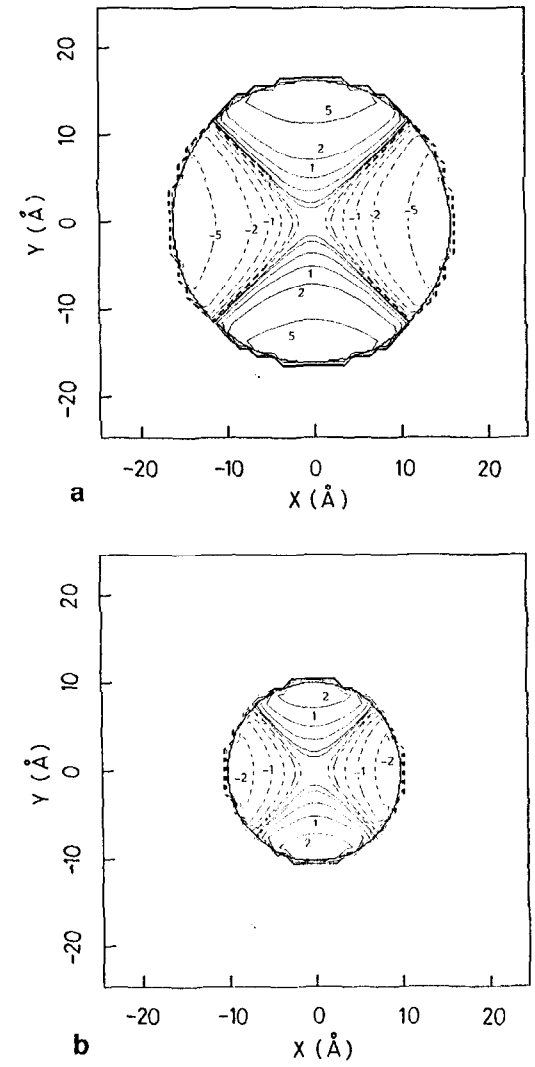

Figure 2. Electrostatic equipotential lines due to the reaction field in the cross section at Z = 0.5 Å *for a quadrupolar dielectric model, where two positive unit charges* +e *were set on the* X*-axis at* X = ±1 Å, *and two negative unit charges* −e *were on the* Y*-axis at* Y = ±1 Å, *in a 16-Å vacuum sphere surrounded by a high dielectric continuum (dielectric constant 80). The meanings of lines and numbers are the same as those in Figure 1:* (a) *The analytical result by the Friedman's equation.*[18] *The bold line is the surface of the vacuum sphere.* (b) *The reproduced potential by the 3 × 1282 pseudo-charges and charge pairs on the closed surface* Γ *(10-Å sphere) with* $\Delta l = 10^{-4}$ Å. *The bold line indicates the surface* Γ.

reaction field potentials of the dipole system. Figures 2a and 2b are those of the quadrupole system. For the reproduction of the reaction field potentials, $3 \times N = 3 \times 1282$ equally spaced pseudo-charges and charge pairs on the surface of the sphere Γ were used, with $\Delta l = 10^{-4}$ Å.

In Figure 3, the relative root-mean-square (rms) differences of the reproduced reaction field potentials from the Friedman's analytical values[18] are indicated for the monopole, dipole, and quadrupole systems. The horizontal axis is the radius of the spherical shell, on which the reaction field potentials were monitored, with 704 equally spaced points for each. It is evident that more than 1.5 Å from the closed surface Γ (10-Å sphere), accuracy better than 1% is obtainable. Even at 1Å from Γ, better than 5% accuracy is obtained.

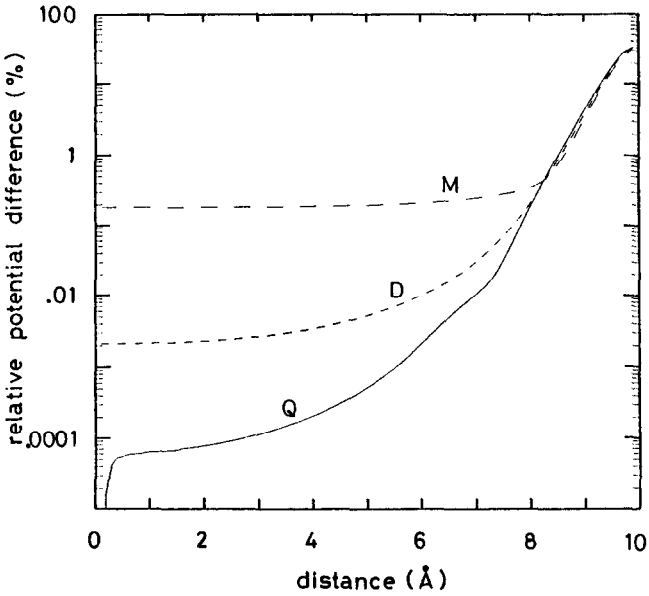

Figure 3. The relative rms difference of the reproduced reaction field potentials from the analytical potentials for the dielectric models described in the text. The dashed line with a character **M** *is for the monopole model, the dotted line with a* **D** *is for the dipole model and the solid line with a* **Q** *is for the quadrupole model. The horizontal axis is the radius of the spherical shell potential values.*

Active site electron structure of Dihydrofolate reductase

For a quantum mechanical analysis of an active site in a protein, it is necessary to incorporate the electrostatic contribution from the whole protein and solvent molecules. The current pseudo-charges and dipoles model is applicable to represent such effects, the origins of which are far from the local QM space.

As an example, the molecular orbital (MO) of the active site ASP 26 side chain of dihydrofolate reductase from *L. casei* (EC 1.5.1.3) and the pteridine ring of its bound inhibitor methotrexate (MTX) was calculated with and without the pseudo-charges and dipoles, which approximate the protein and solvent effects.

First, from the atomic coordinates (PDB code; 3DFR)[19] of the ternary complex of dihydrofolate reductase (DHFR) from *L. casei* with MTX and NADPH, the continuum dielectric model was made with 60 × 60 × 60 small cubic bricks, each side of which was 1 Å. Here, the pteridine ring and the side chain of ASP 26 were artificially separated from the rest part of the MTX and DHFR, respectively. Hereafter, they are called *region I*, as shown in Figure 4. Partial atomic charges of DHFR were taken from the AMBER all-atom force field,[20] and those of MTX and NADPH were taken from the previous QM calculation.[21] Based upon the dielectric model, the electrostatic potential ψ_{total} of the whole system was numerically calculated, solving the finite-difference Poisson–Boltzmann equations following the procedure described previously,[3] with $\kappa_s = 0.1$ Å^{-1}, $\epsilon_0 = 1$, and $\epsilon_s = 80$.

Second, the atoms located inside a 10-Å sphere centered at

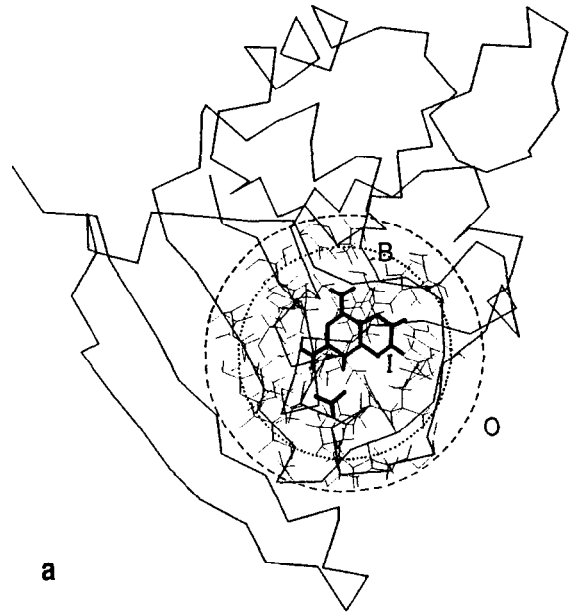

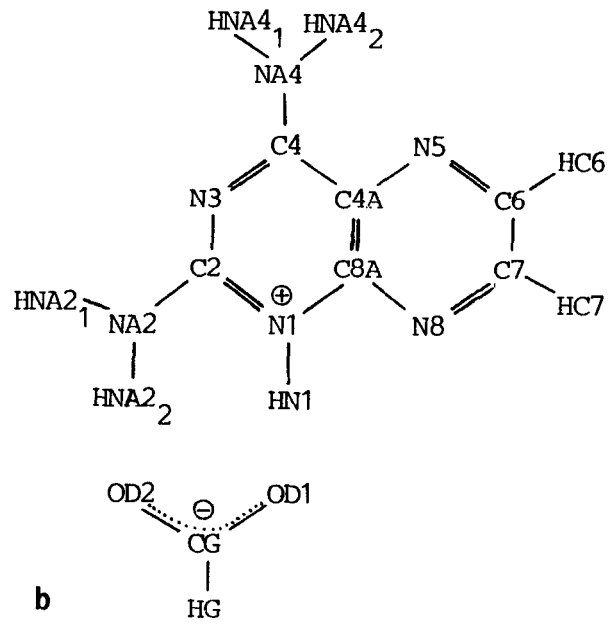

Figure 4. (a) *Partition of the ternary complex of DHFR, MTX, and NADPH into region I for QM calculation, region B for the fixed atoms, and region O for the continuum model. Region I is composed of the pteridine ring of MTX and the side chain of ASP 26 drawn by bold lines. Region B is the inside of a 10-Å sphere, indicated by a dashed circle, that is centered at the N1 atom of the pteridine ring. The atoms in region B are indicated by the thin lines. Region O is the outside of region B. Only backbone C_α atoms of DHFR are shown. The closed surface Γ, on which pseudo-charges and dipoles (or charge pairs) are located, is a 7.5-Å sphere indicated by a dotted line.* (b) *Chemical structure and atom numbering of region I.*

the N1 atom of the pteridine ring, were extracted from the total system. This region, excluding region I is hereafter called *region B*, as shown in Figure 4a. The similar dielectric model composed of regions I and B was made *in vacuo*, and the electrostatic potential ψ^{vac}_{I+B} of this vacuum system was numerically calculated, too. Then, the electrostatic potential φ_0 due to *region O* outside of region B in Figure 4a, was given by subtracting ψ^{vac}_{I+B} from ψ_{total}:

$$\varphi_0 = \psi_{total} - \psi^{vac}_{I+B} \quad (17)$$

The potential φ_0 includes contributions not only from the protein atoms in region O, but also the solvent shielding

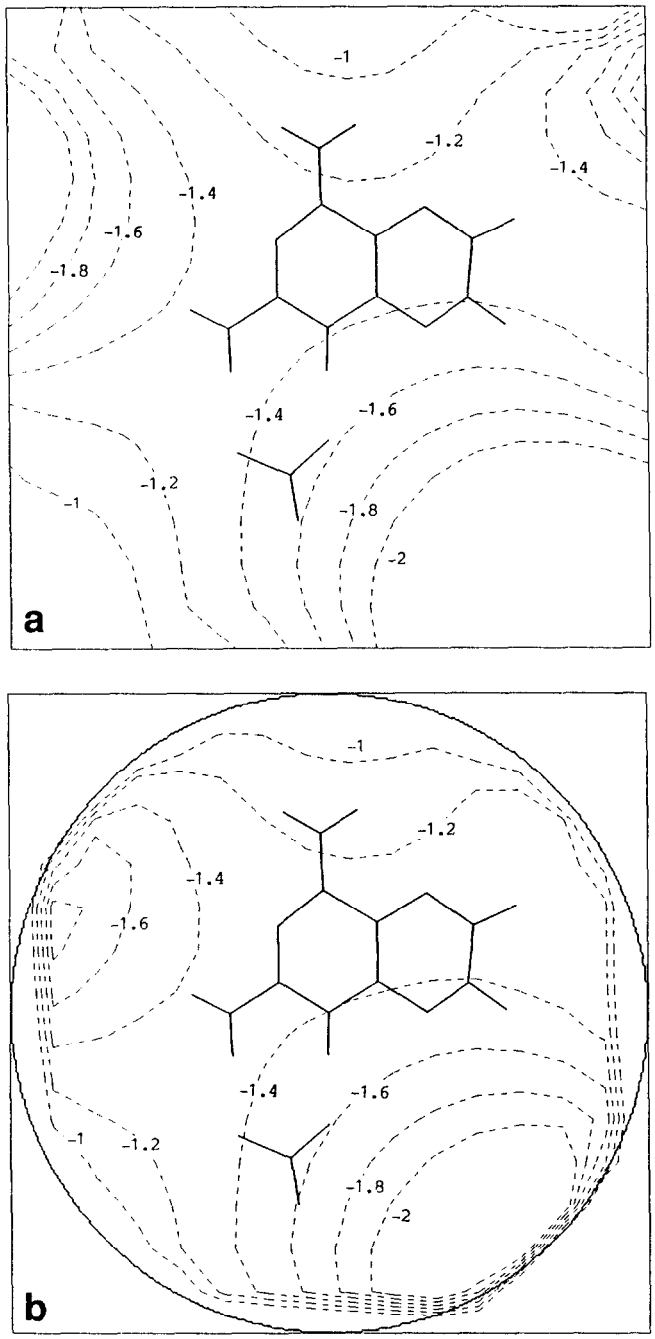

Figure 5. The equipotential lines of φ_0 due to the contribution from region O. The numbers in the figures are the potential values (in V). Region I is shown by the bold lines: (a) *The original mesh potential numerically calculated from a macroscopic dielectric model; $\varphi_0 = \psi_{total} - \psi^{vac}_{I+B}$.* (b) *The reproduced potential by the 3846 pseudo-charges and charge pairs ($\Delta l = 10^{-4}$ Å) on* Γ. *The circle by a bold line indicates the surface of* Γ.

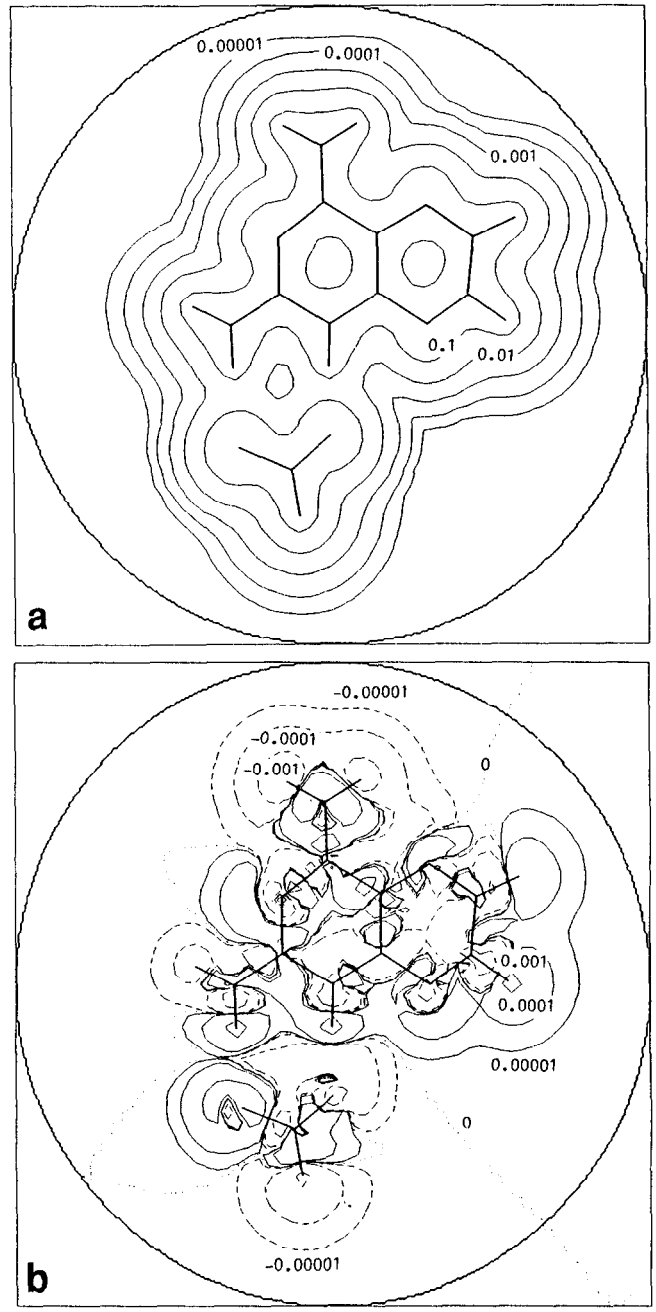

Figure 6. (a) *The electron distribution of region I calculated with the 407 fixed charges in region B and with the 3846 pseudo-charges and charge pairs on* Γ. *The unit of the numbers of the equidensity lines is e/au^3. The circle by a bold line indicates the surface of* Γ. (b) *The difference of the electron distribution of* (a) *from that* in vacuo. *The solid lines are positive, and the dashed lines are negative. The dotted lines indicate zero difference. The unit of the numbers is e/au^3.*

effect, that is, the reaction field effect. The theoretical background of this procedure was previously published.[8] Figure 5a indicates φ_0 around region I.

Third, as described in the preceding section, φ_0 was reproduced by 3×1282 pseudo charges and charge pairs on the 7.5-Å spherical surface centered on the N1 atom of the pteridine. Figure 5b shows the reproduced φ_0. It is also shown in Color Plate 1. The equipotential lines in Figure 5b are similar to those in Figure 5a around the center of the sphere. However, slight differences are observed between Figures 5a and 5b. This is not because of the current algorithm itself, but because of the interpolation procedure to obtain the values of φ_0 and $\nabla\varphi_0$ of Γ from the original mesh potential. On the contrary, the reproduced potential deviated largely from the original potential just near Γ. This is inevitable because of the finite numbers of pseudo-charges and dipoles on Γ, as discussed below.

Finally, the *ab initio* MO calculation for region I was carried out with the 407 atoms (fixed point charges) in region B, and the 3846 pseudo-charges and charge pairs, using the 3-21G* basis set[22] by the program *Gaussian 90*.[23] The electron distribution and its difference from that of region I *in vacuo* are shown in Figures 6a and 6b, respectively. They are also visualized in Color Plates 2 and 3, respectively.

DISCUSSION

As described above, the present algorithm can, in principle, correctly reproduce the potential φ_0 by pseudo-charges and dipoles on an arbitrary closed surface. It gives the inner electrostatic potential straightforwardly by a different approach, using the iterative procedure.[24] In the current examples, only spheres were used as the closed surface, for simplicity. However, other surfaces, such as ellipsoids or polyhedron surfaces frequently used in the finite-element method, are also available.

In numerical calculations, discrete distributions of the pseudo-charges and dipoles of Equations 12 and 13, replacing Equations 9 and 10, give rise to errors, to some extent. As shown in Figures 1, 2, and 5, the reproduced potentials near the closed surface deviated from the original ones. When the number of the surface charges and dipoles becomes smaller, the precision of the reproduced potential decreases, especially near the closed surface. For example, in the case of the reaction field potential due to a dipole, described above, if $N = 200$, the relative rms difference of the reproduced potential from the analytical one is greater than 1% on the spherical shell having a radius larger than 7 Å. When $N = 1282$, the radius for 1% precision is 8.5 Å, as shown in Figure 3.

The error in approximating each pseudo-dipole by a charge pair by Equations 14 and 15 was found to be very small when Δl was taken as a short distance. In the current example of the reaction field potential of the dipole system, the difference between the actual pseudo-dipoles model and the approximated charge pairs model was less than 10^{-2}% and 10^{-6}% for $\Delta l = 0.01$ Å and 0.0001 Å, respectively, inside the 9.9-Å monitoring sphere. This means that for small Δl, one can almost completely approximate the contribution from each point dipole by a charge pair.

In the application to the combination of the *ab initio* MO calculation and the continuum dielectric model, the reaction field effect due to region I was included in φ_0. That is, the procedure should be iterative. One may worry about whether the procedure converges. In the current calculation, the rms difference of the Mulliken population on each atom in region I from that calculated *in vacuo* was as small as 0.0146 *e*. Therefore, one or two iterations seems enough for the convergence, because the high dielectric solvent region is far from region I at present.

In this article, one application of the *ab initio* MO calculation has been shown to incorporate the protein and solvent effect by the present algorithm. To an analysis of the electronic structure of a much more complicated system, such as the chlorophyll dimer in the photosynthetic reaction center,[25] this approach can be applied for considering the influence of the surrounding proteins.

Other applications are available not only for such static models, but also for dynamic systems. For instance, when a MD calculation for a protein in aqueous solution is carried out, the effect of the solvent far from the protein can be reproduced by pseudo-charges and dipoles in an averaged manner. This is a modified approach of the previous method[26,27] to combine the reaction field potential by the continuum model with the MD calculation.

In the other application combining QM calculation with MD, instead of with the continuum dielectric model, the potential in the QM region due to the classical region may be given as the average of a long-run result of a classical MD calculation. The long-distance effect can be represented as an average by pseudo-charges and dipoles on an arbitrary surface surrounding the quantum region. Then, a QM calculation is carried out with the MD calculation in the border region, similar to the recent procedure developed by Field *et al.*,[17] but with the additional pseudo-charges and dipoles.

ACKNOWLEDGMENTS

All calculations were performed using FACOM VP-400E (Fujitsu) at Protein Engineering Research Institute. The author thanks Mr. K. Teraishi for the usage of *Gaussian 90*.

REFERENCES

1 Warshel, A. and Russell, S.T. Calculation of electrostatic interactions in biological systems and in solutions. *Q. Rev. Biophys.* 1984, **17**, 283–422
2 Warwicker, J. and Watson, H.C. Calculation of the electric potential in the active site cleft due to α-helix dipoles. *J. Mol. Biol.* 1982, **157**, 671–679
3 Nakamura, H. and Nishida, S. Numerical calculations of electrostatic potentials of protein-solvent systems by the self-consistent boundary method. *J. Phys. Soc. Jap.* 1987, **56**, 1609–1622
4 Gilson, M.K. and Honig, B.H. Calculation of electrostatic potentials in an enzyme active site. *Nature* 1987, **330**, 84–86
5 Sternberg, M.J.E., Hayes, F.R.F., Russell, A.J., Thomas, P.G., and Fersht, A.R. Prediction of electrostatic effects of engineering of protein charges. *Nature* 1987, **330**, 86–88
6 Takahashi, T., Nakamura, H., and Wada, A. Electrostatic forces in two lysozymes: Calculations and measure-

ments of two histidine pKa values. *Biopolymers* 1992, **32**, 897–909
7 Nakamura, H., Sakamoto, T., and Wada, A. A theoretical study of the dielectric constant of protein. *Protein Engineer.* 1988, **2**, 177–183
8 Nakamura, H. Numerical calculation of reaction fields of protein-solvent systems. *J. Phys. Soc. Jap.* 1988, **57**, 3702–3705
9 Eastwood, J.W., Hockney, R.W., and Lawrence, D.N. P3M3DP—The three-dimensional periodic particle–particle/particle–mesh program. *Comput. Phys. Comm.* 1980, **19**, 215–261
10 Warshel, A. and Levitt, M. Theoretical studies of enzymatic reactions: dielectric, electrostatic and steric stabilization of the carbonium ion in the reaction of lysozyme. *J. Mol. Biol.* 1976, **103**, 227–249
11 Warshel, A. and Weiss, R.M. An empirical valence bond approach for comparing reactions in solutions and in enzymes. *J. Am. Chem. Soc.* 1980, **102**, 6218–6226
12 Weiner, S.J., Seibel, G.L., and Kollman, P.A. The nature of enzyme catalysis in trypsin. *Proc. Natl. Acad. Sci. USA* 1986, **83**, 649–653
13 Reynolds, C.A., King, P.M., and Richards, W.G. Computed redox potentials and the design of bioreductive agents. *Nature* 1988, **334**, 80–82
14 Rullmann, J.A.C., Bellido, M.N., and van Duijnen, P. Th. The active site of papain: All-atom study of interactions with protein matrix and solvent. *J. Mol. Biol.* 1989, **206**, 101–118
15 Richards, W.G., King, P.M., and Reynolds, C.A. Solvent effects. *Protein Engineer.* 1989, **2**, 319–327
16 Singh, U.C. and Kollman, P.A. A combined *ab initio* quantum mechanical and molecular mechanical method for carrying out simulations on complex molecular systems: Applications to the $CH_3Cl + Cl^-$ exchange reaction and gas phase protonation of polyethers. *J. Comput. Chem.* 1986, **7**, 718–730
17 Field, M.J., Bash, P.A., and Karplus, M. A combined quantum mechanical and molecular mechanical potential for molecular dynamics simulations. *J. Comput. Chem.* 1990, **11**, 700–733
18 Friedman, H.L. Image approximation to the reaction field. *Mol. Phys.* 1975, **29**, 1533–1543
19 Bolin, J.T., Filman, D.J., Matthews, D.A., Hamlin, R.C., and Kraut, J. Crystal structures of *Escherichia coli* and *Lactobacillus casei* dihydrofolate reductase refined at 1.7-Å resolution. *J. Biol. Chem.* 1982, **257**, 13650–13662
20 Weiner, S.J., Kollman, P.A., Nguyen, D.T., and Case, D.A. An all-atom force field for simulations of proteins and nucleic acids. *J. Comput. Chem.* 1986, **7**, 230–252
21 Komatsu, K., Nakagawa, S., Umeyama, H., and Nakamura, H. Electrostatic interaction energy and solvent accessibility in the methotrexate-reduced nicotinamide adenine dinucleotide phosphate-dihydrofolate reductase ternary complex. *Chem. Pharm. Bull.* 1987, **35**, 1880–1895
22 Pietro, W.J., Francl, M.M., Hehre, W.J., DeFrees, D.J., Pople, J.A., and Binkley, J.S. Self-consistent molecular orbital methods. 24. Supplemented small split-valence basis sets for second-row elements. *J. Am. Chem. Soc.* 1982, **104**, 5039–5048
23 Frisch, M.J., Head-Gordon, M., Trucks, G.W., Foresman, J.B., Schlegel, H.B., Raghavachari, K., Robb, M., Binkley, J.S., Gonzalez, C., DeFrees, D.J., Fox, D.J., Whiteside, R.A., Seeger, R., Melius, C.F., Baker, J., Martin, R.L., Kahn, L.R., Stewart, J.J.P., Topiol, S., and Pople, J.A. *Gaussian 90, Revision H,* Gaussian, Inc., Pittsburgh, PA 15213, 1990
24 Pascual-Ahuir, J.L., Silla, E., Tomasi, J., and Bonaccorsi, R. Electrostatic interaction of a solute with a continuum. Improved description of the cavity and of the surface cavity bound charge distribution. *J. Comput. Chem.* 1987, **8**, 778–787
25 Sakuma, T., Takada, T., Kashiwagi, H., and Nakamura, H. *Ab initio* MO calculations of the chlorophyll dimer in the photosynthetic reaction center. *Int. J. Quant. Chem., Quant. Biol. Symp.* 1990, **17**, 93–101
26 Nakamura, H. Theoretical calculations of electrostatic effects in biological macromolecules. *5th FAOB Symposium in Seoul,* 1989
27 Sharp, K. Incorporating solvent and ion screening into molecular dynamics using the finite-difference Poisson–Boltzmann method. *J. Comput. Chem.* 1991, **12**, 454–468